
Using Learning Dynamics to Explore the Role of Implicit Regularization in Adversarial Examples

Josue Ortega Caro

Department of Neuroscience
Baylor College of Medicine
Houston, TX, 77030
caro@bcm.edu

Yilong Ju

Department of Computer Science
Rice University
Houston, TX, 77005
yilongju@rice.edu

Ryan Pyle

Department of Neuroscience
Baylor College of Medicine
Houston, TX, 77030
rpyle@bcm.edu

Ankit B. Patel

Department of Electrical and Computer Engineering
Rice University
Houston, TX, 77005
abp4@rice.edu

Abstract

Recent work [11] suggests that adversarial examples are “features not bugs”. If adversarial perturbations are indeed useful but non-robust features, then what is their origin? In order to answer these questions, we systematically examine the learning dynamics of adversarial perturbations both in the pixel and frequency domains. We find that: (1) adversarial examples are not present at initialization but instead emerge very early in training, typically within the first epochs, as verified by a novel breakpoint-based analysis; (2) the low-amplitude high-frequency nature of common adversarial perturbations in natural images is critically dependent on an *implicit bias towards sparsity in the frequency domain*; and (3) the origin of this bias is the locality and translation invariance of convolutional filters, along with (4) the existence of useful frequency-domain features in natural images.

We provide a simple theoretical explanation for these observations, providing a clear and minimalist target for theorists in future work. Looking forward, our findings suggest that analyzing the learning dynamics of perturbations can provide useful insights for understanding the origin of adversarial sensitivities and developing robust solutions.

1 Introduction

Despite the enormous progress in training neural networks to solve hard tasks, they remain surprisingly and stubbornly sensitive to imperceptibly small worst-case perturbations known as *adversarial examples*. This lack of robustness has sparked many theories [6, 14, 22, 4, 3, 2, 8, 20] but together they fail to explain many perplexing observations. Compelling recent work [11] has illuminated the situation greatly by proposing the ‘Features-Not-Bugs’ (FNB) hypothesis, which states that adversarial sensitivity is a simple consequence of state-of-the-art models learning well-generalizing features in the dataset. From the FNB perspective, since models are trained only for maximizing accuracy, they have the freedom to choose useful but non-robust features that humans find non-intuitive.

What is the nature of these features? Recent work[27] proposes the High Frequency (HF) hypothesis, which states that state-of-the-art classifiers are using low amplitude, high frequency features in natural images. Given the strong theoretical connection between adversarial features and perturbations in

linear models[7], it stands to reason that we should expect a similarly strong relationship in nonlinear models. In this vein, [27] also finds that adversarial perturbations of naturally trained models tend to be higher frequency. In contrast, those of *adversarially* trained models tend to be lower frequency, explaining several otherwise perplexing tradeoffs seen in corruption-based data augmentation studies [27, 18]. Though not all adversarial features are high frequency [27], understanding the origin of high frequency features is an important step towards building robust, interpretable models.

In this paper we propose the Implicit Fourier Regularization (IFR) hypothesis, which claims that:

Implicit regularization in frequency domain, directly caused by the translation invariance of the convolution operation, is necessary for the evolution of high frequency adversarial perturbations.

Through systematic experiments examining the learning dynamics of deep linear and nonlinear models, we provide strong empirical support for this claim, along with theoretical support in the case of deep linear models.

Main Contributions Our main contributions are as follows. First, by exploring learning dynamics, we confirmed the “Features not Bugs” Hypothesis. Second, based on extensive, systematic experiments, we propose the *Implicit Fourier Regularization Hypothesis*: that the frequency-driven nature of adversarial examples for real-world deep networks originates from an implicit bias towards sparsity in the Fourier domain, which in turn is caused by the translation invariance of convolutions. We extend the theory of [9] to bounded-width convolutions in this regard, and we find that the *radial distribution of energy* in the frequency spectrum of the adversarial perturbation reveals the different implicit biases induced by various architectures and weight initializations.

2 Related Work

Explanations of Adversarial Examples. Several papers have tried to understand the conditions that are necessary for sensitivity to adversarial noise. Some work has focused on statistical properties of the data distribution [6, 14, 22, 4, 3], whereas others have studied overfitting or underfitting as the key property [2, 8, 20]. See [11] for an comprehensive review. However, to our knowledge no existing work has used learning dynamics nor implicit regularization theory as a way to understand adversarial development.

Fourier Analysis of Input Perturbations. Recent work on robustness to adversarial and noise perturbations has used a Fourier perspective to understand how various data augmentation techniques can make different models more robust [11, 18]. In [11] the authors have found that adversarial training and other forms of noise perturbations produce models which are robust to high frequency noise. With this knowledge, they have designed better noise generation and data augmentation techniques. Our work tries to explain why adversarial examples of convolutional neural network evolves in frequency space compared to other models.

Relationship between Performance and Adversarial Attacks. Some papers have study the relationship between performance and adversarial development. In [21] the authors have established that for certain loss functions, adversarial examples are inescapable and that input complexity could affect the robustness of the model. In addition, [11, 26, 23, 16] have found that for classification problems adversarial examples improve the performance of the classifier, and that adversarial robustness is at odds with accuracy.

Theories of Learning Dynamics & Implicit Regularization. This line of theoretical work aims to understand how *overparameterized* neural nets with more parameters than training data can possibly generalize [24, 9, 5, 25]. Early work revealed the surprising phenomenon of *implicit regularization*: When a loss surface possesses many *global* minima of equal value, which is common in overparametrized models, the specific global minima that a learning algorithm converges to can depend greatly on seemingly idiosyncratic details such as the choice of parameter initialization scheme, specific learning algorithm, or architecture. Recent studies have also shown that such implicit bias/regularization is responsible for much if not most of the generalization performance of state-of-the-art image classifiers[13, 1]. Our paper specifically utilizes recent work[9] that shows that overparametrized deep linear models with and without convolutions induce dramatically different implicit biases, the former yielding a bias towards sparsity in the *Fourier* domain. In Section 3.3.1 we

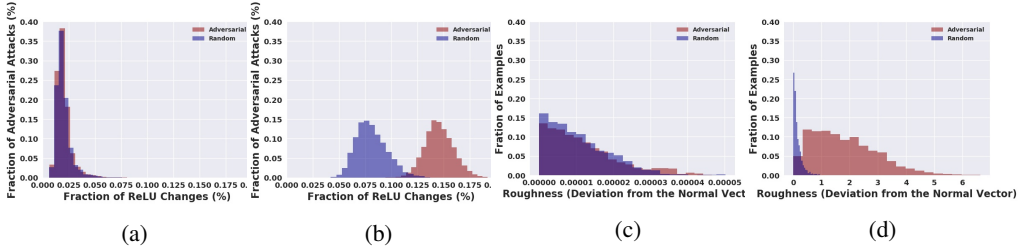


Figure 1: Testing the Features not Bugs (FNB) Hypothesis. Left: Distribution of ReLU Changes (Metric for Breakpoint movement) for (a) initial and (b) final ResNet18 model along perturbation from original to adversarial/random images. Right: Distribution of Roughness (Metric for Curvature) for (c) initial and (d) final ResNet18 Model along same perturbations. Both ReLU Changes and Roughness start the same for both perturbations, but increase more by the end of training for the adversarial perturbations.

hypothesize that such *implicit Fourier regularization*, combined with useful features in the dataset, are necessary for the emergence of sparse high frequency adversarial examples during learning.

3 Empirical Study of Learning Dynamics

3.1 Learning Dynamics supports Features-Not-Bugs Hypothesis

Breakpoints migrate to Adversarial Directions at a far higher rate than Random Directions.

To further understand and test the FNB hypothesis, we used function space theory developed for ReLU Neural Networks that re-parametrizes the latter as continuous piecewise linear (CPWL) spline functions with breakpoints/breakplanes (where slope changes discontinuously) and delta-slope parameters (the magnitude of the change in slope along a particular direction) [24, 19]. From the spline perspective, modeling curvature in the target function necessitates the flow of breakpoints from their initial locations (determined by the weight initialization) to regions of high curvature. The theory has been successful in explaining several otherwise perplexing phenomenon including the need for overparametrization in training, the structure of the loss surface, the Hessian spectrum’s correlation with smoothing, and implicit regularization.

Motivated by this theory, our interest in adversarial examples, and the "features not bugs" (FNB) hypothesis, a natural question is: To what degree do adversarial attacks take advantage of input directions that already have a preexisting high density of breakpoints? Or do breakpoints only move during training to functionally relevant directions that then are utilized by the adversarial attack?

In order to test this, we trained a ResNet18 model on the CIFAR-10 dataset. After training, we used the Foolbox package [17] to generate adversarial attacks for every example in the test set via an ℓ_∞ Projected Gradient Descent attack [12] (see Sec. B.4). Once we had the adversarial examples, we pass both the original and adversarial images through the intermediate models (saved during training) and measured two observables along the line connecting the original x and adversarial $x_a := x + \delta$ image: (1) Changes in binary ReLU states (active to inactive or vice versa); and (2) the change in curvature in the logits for correct and adversarial categories. Then we compare both of these metrics to a noise-perturbed example image $x_r := x + r$ with the same norm as the adversarial example ($\|x_a\| = \|x_r\|$), but perturbed in a different *random* direction $r \sim \mathcal{N}(\mathbf{0}, \mathbf{1})$.

In Figure 1a,b, we can see that the distribution of the fraction of ReLU changes for the both random and adversarial directions is the same at the beginning of training but then diverges significantly by the end. Furthermore, in Figure 1c,d, we can see that the distribution of roughness (Measured as the deviation from the normal vector) per example along the adversarial direction increases through time and diverges for adversarial vs random perturbations. This can also be seen for intermediate models (Sup. Figure 6).

Success of Adversarial Attacks early in training is correlated with Classification Accuracy.

To further test the FNB hypothesis, we ask: Does the development of adversarial examples during training correlate with gains in accuracy? To answer this we select model snapshots from intermediate times during training and perform adversarial attacks on them. We considered an adversarial attack to be successful if the original image was correctly classified by the model *and* if the adversarial

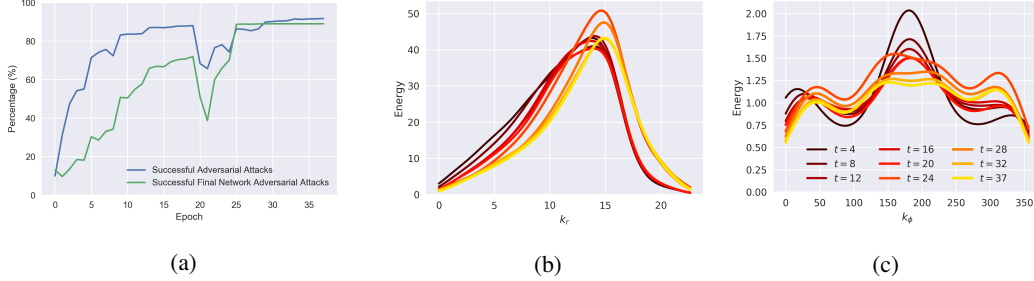


Figure 2: (a) Successful Final Network Adversarial attacks lag behind Successful Attacks on intermediate models. Performance lag suggests that the nature of the adversarial attacks changes during training. (b) Distribution of radial energy k_r of the Fourier spectrum of adversarial perturbations. (c) Distribution of angular energy k_ϕ (in degree) of the Fourier spectrum of adversarial perturbations. (b,c) show an evolution of adversarial perturbations over training from lower to higher frequencies for the ResNet18 model, and from certain directions to all directions uniformly.

example was within a Euclidean distance of ϵ , *i.e.*, $\|x_a - x\| \leq \epsilon$, as defined by the attack (Supp. Sec. B.4).

Figure 2 shows that the *adversarial success rate*, defined as the percentage of examples for which a successful adversarial attack was found, increased by the same amount as the training/test accuracy. This suggests that adversarial examples develop in the model as performance increases, further supporting the FNB hypothesis. However, we also see that the adversarial examples computed for the final network after training lag behind in performance compared to the adversarial attack computed for intermediate models (Figure 2). This indicates that the final network’s adversarial attacks are not fully transferable to the intermediate networks. This raises the question: Does the *nature* of the adversarial attacks change during the course of learning?

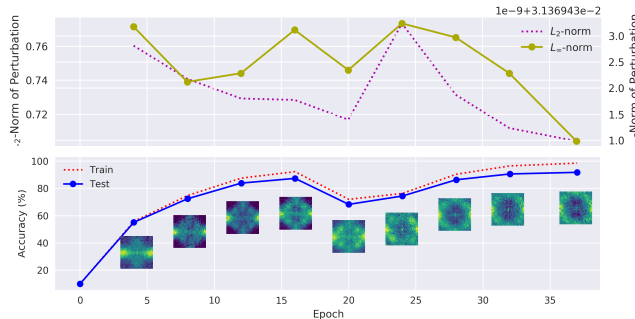


Figure 3: Top: Dynamics of L_2 and L_∞ Norms of the Adversarial Perturbations (δ) during training for ResNet18. As training occurs, adversarial attacks become smaller in amplitude. Bottom: Evolution of the Adversarial Perturbation Spectrum ($\hat{\delta}$) during training. Adversarial Perturbation Spectrum evolves from low-frequency attacks to high frequency attacks as performance increases.

Minimum Distance Adversarial Features Change throughout Learning. One of the most important defining properties of adversarial examples is that they have low norm and are thus typically imperceptible by eye. Are adversarial attacks low norm *throughout* training? We measured the norm $\|\delta\|$ of the adversarial perturbation δ during learning, using the ℓ_2 and ℓ_∞ norms. Figure 3 (Top) shows us that both $\|\delta\|_2$ and $\|\delta\|_\infty$ norms decrease during training, showing that low norm perturbations *require* training well.

3.2 Dynamics of Adversarial Examples in Frequency Domain

Energy in Adversarial Perturbations flows from Low to Medium/High Frequencies Are adversarial perturbations simply changing in norm, or do they also change *in direction* during training? To test this, we took inspiration from [27] and adopted a Fourier perspective. Their work suggests that

networks trained for adversarial robustness tend to be robust to high frequency perturbations and so we decided to study the learning dynamics of adversarial perturbations in the frequency domain.

As with previous experiments, we performed adversarial attacks on intermediate models \mathcal{M}_t during training, and measured the 2-D Discrete Fourier spectrum $\widehat{\delta}_t := \mathcal{F}\delta_t$ of the perturbation δ_t . In Figure 3 (Bottom), we see that early on in training the adversarial perturbations tend to contain low frequencies. As training progresses, we see the evolution towards higher frequencies. Thus as training progresses, adversarial perturbations contain more and higher frequencies with lower amplitudes (decrease in $\|\delta_t\|$ over time). This can also be observed in Figures 2b and 2c, where we show the marginal radial and angular distributions $E(k_r), E(k_\phi)$ of the energy spectrum $E(k_r, k_\phi) := |\widehat{\delta}(k_r \cos k_\phi, k_r \sin k_\phi)|_{\mathbb{C}}^2$, where (k_r, k_ϕ) denote polar coordinates in the frequency domain. We also observe that (i) the radial energy distribution shifts from low to high frequency k_r , and (ii) the angular energy distribution becomes more uniform, corresponding to the observed ring structure.

3.3 Implicit Regularization in Frequency Domain impacts Adversarial Perturbations

Recent theoretical work [9, 24, 19] has shown that learning dynamics – influenced by the choice of model parametrization, weight initialization scheme, and gradient descent-based optimization algorithm – plays a pivotal role in the generalization performance of deep networks[1] by inducing an *implicit* model bias in the form of regularization. This implicit bias depends critically on the choice of parametrization, sparking much recent work attempting to characterize the implicit bias/regularizer for various popular (or analytically tractable) architectures and learning algorithms. In particular, [9] shows that shallow linear convnets with a single hidden layer (1 full-width circular convolutional linear layer followed by 1 fully connected linear layer) induce an implicit sparsity-promoting regularizer in the Fourier domain *i.e.*, $\mathcal{R}_{CONV}(\beta) = \|\widehat{\beta}\|_1$ where $\widehat{\beta} := \mathcal{F}\beta$ is the Discrete Fourier Transform (DFT) of the end-to-end linear transformation $\beta := W_2W_1$ represented by the linear network. Furthermore the sparsity promotion intensifies with increasing depth yielding an implicit regularizer $\mathcal{R}_{CONV,L}(\beta) = \|\widehat{\beta}\|_{2/L}$ where L is the number of hidden convolutional layers.

In stark contrast, they find that a *fully connected* linear network with a single hidden layer (2 fully connected linear layers) induces a *ridge* regularizer $\mathcal{R}_{FC}(\beta) = \|\beta\|_2^2$ in the pixel or space domain. Furthermore, this regularization does not change with depth *i.e.*, $\mathcal{R}_{FC,L}(\beta) = \|\beta\|_2^2$. Based on this we state our main hypothesis: *that convolutions induce an implicit Fourier regularization that strongly impacts the frequency spectra of adversarial perturbations.*

Recent theoretical work in this space focuses mostly on linear models and so our first step is to test this hypothesis in linear models. Furthermore, given the complexity of modern architectures and learning algorithms, we also ask: What are the *minimal conditions* (architecture type, hyperparameters, dataset, etc.) that are required for different kinds of biases in adversarial examples to form? This approach enables us to use linear learning dynamics theory to better understand the origin of adversarial features and their dependence on model parameterization. Armed with our linear understanding, we can then empirically explore nonlinear models like the ResNet18 model used for our earlier analysis.

3.3.1 Exploring Linear Models: Testing the Implicit Regularization Theory and expanding to Bounded-Width Convolutions

Fully Connected vs Full-Width Convolutional Models show different implicit bias in the frequency domain, as predicted by Implicit Fourier Regularization Theory[9]. In order to test the implicit Fourier regularization (IFR) theory, we first trained a 1 hidden layer linear fully connected model and a 1 layer hidden linear 3-channels (circular full-width) convolutional model on CIFAR-10. Both models achieved similar test accuracies (Supp. Table 4)

In Figure 8a, we visualize the linear classifier (end-to-end weights) for the chosen class $\beta := \beta_{c_n}$, the adversarial perturbation δ , and their respective Fourier spectra $\widehat{\beta}$ and $\widehat{\delta}$ for the fully connected and convolutional linear models. We observe that $\widehat{\beta}$ for the Full Width Convolution model is more sparse compare to the Fully Connected model which is also reflected in the $\|\widehat{\beta}\|_1$ (Figure 5) and in the radial distribution of energy (Figure 8b). This indicates that both models conform to the predictions from IFR theory in [9], and that there is a direct relationship between β and δ . Furthermore, the IFR Theory states that this difference should increase with depth. In Figure 5, we see that a deep full width convolutional model yields a smaller $\|\widehat{\beta}\|_1$ than the shallow full width convolutional model,

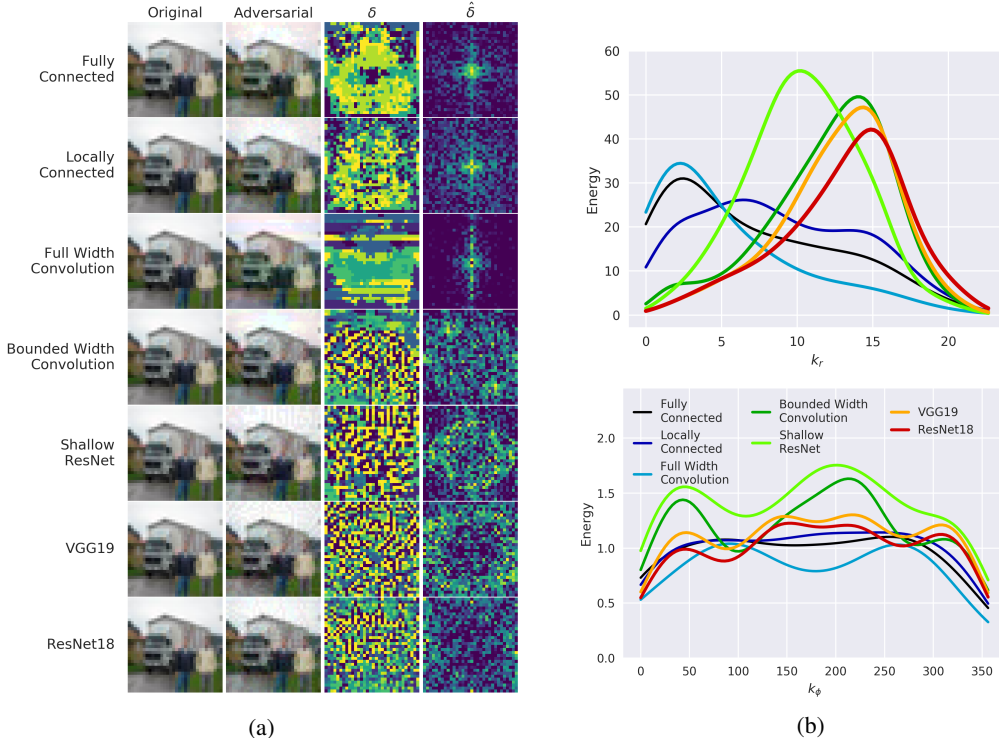


Figure 4: (a) Example Visualization of δ and $\hat{\delta}$ for 5 nonlinear models with one hidden layer and 2 deep nonlinear networks. We observe qualitatively that both full width convolutional model have sparse frequency spectrum, as compared to the Fully Connected and Locally Connected models (For quantification, Table 5 and Supp Figure 10). (b) Radial (top, k_r) and Angular (bottom, k_ϕ in degree). Distribution of Energy in $\hat{\delta}$ show that deep, bounded-Width models shift energy into higher frequencies, and the angular energy of Fully Connected and Locally Connected models are distributed more uniformly.

but that no such depth dependence exists for a 3 hidden layer fully connected vs 1 hidden layer fully connected. Finally, Supp. Figure 9) shows that this behavior is not specific to one image but is indeed present in the average Fourier spectrum of the adversarial perturbations for both fully connected and full width convolutional models.

Increasing the Number of Channels and restricting to Bounded-Width Convolutions Concentrates Energy in Higher Frequencies. Given that the IFR theory[9] applies only to full-width circular convolutions with equal number of hidden units as their input, we asked: does a similar bias occur in bounded-width and multi-channel convolutions? In Figure 5, we observe that a 3-channel 3×3 kernel linear convolutional model is not less dense than its full-width counterpart, but does show more concentration in higher frequencies than a Fully Connected model (Supp. Figures 9, 8b). This is likely due to the additional spatial constraints imposed on the bounded-width convolutions which, via the Fourier Uncertainty Principle (a space-limited kernel *cannot* be band-limited in Fourier domain), drive frequency dispersion in the Fourier domain. *This frequency dispersion is in tension with the sparsity promotion predicted by the IFR theory, resulting in a compromise sparsity that is lower than that of the full-width convolutional model.* This intuition can be made rigorous for a 3-channel bounded-width linear convolutional model, extending the results of [9], as follows.

Lemma 1. *For full-width convolutional networks, let the parametrization map be $\mathcal{P}_{CONV}(\mathbf{w}) = \left(((\mathbf{w}_L^\downarrow \star \mathbf{w}_{L-1}) \star \mathbf{w}_{L-2}) \dots \star \mathbf{w}_1 \right)^\downarrow$, where \mathbf{w}^\downarrow denotes the flipped vector corresponding to \mathbf{w} , given by $\mathbf{w}^\downarrow[k] = \mathbf{w}[D - k - 1]$ for $k \in [D]$. Furthermore let $\mathcal{C}_{l,d} := \{\mathbf{w}_l \in \mathbb{R}^{D_l} : \mathbf{w}_l[i] = 0 \forall i \notin [d]\}$ be the convex constraint set of bounded width (or spatially limited) filters. Then for a depth L bounded width d (a.k.a. locally connected) linear convolutional network with parameters*

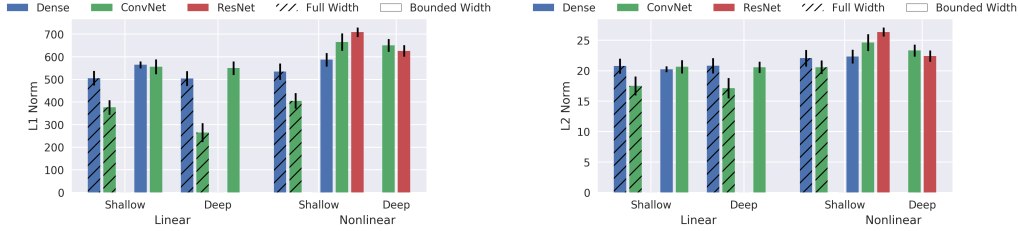


Figure 5: Comparison of Adversarial Perturbation Norms $\|\hat{\delta}\|_p$ for $p = 1, 2$ for different linear and nonlinear models. The relations between norms of nonlinear models mirror and accentuate those of linear models. See Sections 3.3.1–3.3.2 for detailed comparisons.

$\mathbf{w} = [\mathbf{w}_l \in \mathbb{R}^D]_{l=1}^L$ and parameterization map $\mathcal{P}_{BWC\text{ONV}}(\mathbf{w})$, the implicit regularizer is

$$\mathcal{R}_{\mathcal{P}_{BWC\text{ONV}}}(\beta) = \min_{\mathbf{w}: \mathcal{P}_{\text{CONV}}(\mathbf{w})=\beta} \|\mathbf{w}\|_2^2 \text{ s.t. } \mathbf{w}_l \in \mathcal{C}_{l,d} \forall l \in [L].$$

Remark. Note that in the special case of a full-width convolution the implicit regularizer reduces to $\mathcal{R}_{\mathcal{P}_{BWC\text{ONV}}}(\beta) = \min_{\mathbf{w}: \mathcal{P}_{\text{CONV}}(\mathbf{w})=\beta} \|\mathbf{w}\|_2^2 = \|\hat{\beta}\|_1$, as expected from [9]. In the general case, since each convolutional filter \mathbf{w}_l is constrained to be bounded-width (or spatially limited), we can apply the Fourier Uncertainty Principle to get that its frequency spectrum *cannot* be bounded-width (or equivalently, *cannot* be band limited) *i.e.*, $\Delta(\hat{\mathbf{w}}_l) \geq 1/\Delta(\mathbf{w}_l) = O(1/d)$ where $\Delta(\cdot)$ is a reasonable measure of spread (*e.g.*, standard deviation) in the set of filter weights.

Increasing the Number of Channels. In practice, most convolutional models have an expansion from the input to hidden layer, so we asked: What is the effect of varying the number of channels on δ . We expanded the previous bounded width model to 32 channels, and we observe that this model exhibits more spread across all frequencies than the 3-channel model (Supp. Figure 9). We hypothesize that for the linear model increasing the number of filters creates a more dense representation which amplifies the energy in all frequencies.

Finally, in Sup. Figures 8a,b, we found that a 3 hidden layer 32-channel bounded convolutional model produces energy in low and high frequencies, but with decreasing energy in medium frequencies. In addition, the Fourier spectrum of the adversarial perturbations also show more energy in the low and high frequencies (Supp. Figure 9). This indicates that even in a deep bounded width convolutional model there is a tension between the sparsity induced by the implicit Fourier regularizer and the frequency dispersion induced by bounded width. In addition, it shows that β and δ are strongly linked.

Translation Invariance is Necessary for Sparsity in $\hat{\beta}$ and $\hat{\delta}$. Is local connectivity sufficient for this behavior? Or do we need translation invariance? We trained a linear locally connected model with 3×3 kernels and a single hidden layer. In Figure 1b, we see that the Fourier spectrum of the β for the locally connected model has $\|\hat{\beta}\|_1$ similar to the bounded-width convolutional model, but energy is spread across all frequencies, similar to a fully connected model (Supp. Figure 9). This indicates that translation invariance is a necessary component for inducing the implicit Fourier bias during learning.

Initial Weight Scale strongly impacts Implicit Regularization. In addition to the parametrization, previous work [25] has shown that the scale of the initial weights, denoted α , also determines the nature of implicit regularization in overparameterized linear models, with $\alpha \gg 1$ yielding the ridge regularizer $\|\beta\|_2$ and $\alpha \ll 1$ yielding the lasso regularizer $\|\beta\|_1$. Motivated by this result, we investigate the impact of initial weight scaling in the locally connected and convolutional linear models for $\alpha \in \{0.1, 1, 10\}$. In Supp. Figures(11a,11b), we observe that high α induces sparse, higher frequency adversarial attacks for both the locally connected and convolutional linear models, although only the latter exhibits ring structure in its spectrum. This further shows that the choice of initial weight scale strongly impacts the implicit regularizer, and that convolutions seem necessary for inducing frequency-specific attacks.

3.3.2 Nonlinear Models Mirror Theoretical and Experimental Results from Linear Models

Given the results obtained on linear models, we next explore the impact of higher expressive power by investigating nonlinear models. For systematic comparison, we use the same shallow architectures defined in Section 3.3.1 and add nonlinear Rectified Linear Units (ReLUs). Due to their higher expressive power, these models achieve higher accuracy than their linear counterparts (Supp. Table 4).

Nonlinear Model intensify translation Invariance bias for Frequency-driven Adversarial Examples First, we compared the (nonlinear) Fully Connected model to the Full Width Convolutional model, and we observe that the latter has a smaller $\|\hat{\delta}\|_1$ norm than the former (Figure 5), consistent with results observed with the corresponding linear models. This further supports our implicit Fourier regularizer hypothesis.

Next, we tried to evaluate if the bounded width convolutional model presents more power in high frequencies, and if the locally connected model shows spread across all frequencies (as seen in their linear counterpart). In Supp. Figure 10, we observe that the bounded model has more energy in the frequency spectrum of the adversarial perturbation than the full width convolutional model and the fully connected model. This relationship is more amplified than the that observed between the linear counterparts. This difference is further observed in the energy distribution of the adversarial perturbations (Figure 4b). In contrast to these results, the nonlinear locally connected model has a $\hat{\delta}$ similar to the fully connected model, not showing the large energy spread present in the linear model (Supp. Figure 10, 4b).

Thus, the results/relations obtained from the nonlinear models mirror and accentuate the various results/relations obtained from the linear models: for example, translation invariance is necessary for sparsity in the Fourier spectrum of adversarial attacks. Furthermore, bounded width convolutional models seem to exhibit a competition between the implicit Fourier regularizer and the frequency dispersion due to the Fourier Uncertainty Principle. This shows that the implicit regularization induced by the choice of parametrization still has a strong impact on adversarial perturbations in *nonlinear* models.

Adversarial Spectra of Shallow ConvNet and ResNet Differ Greatly. Does this phenomenon change in more complex state-of-the-art models like Resnets[10]? Previous work [15] suggests that deep ResNets are able to capture more high frequency information from inputs than deep ConvNets, controlling for depth and the number of nonlinearities. Does a similar relationship hold for shallow ResNets and convolutional models? In order to test this we trained a shallow ResNet model on CIFAR-10, and as expected it achieves the highest performance amongst all shallow nonlinear models (Figure 4). In Table 2, we observe that $\|\hat{\delta}\|_2$ and $\|\hat{\delta}\|_1$ of the ResNet Model are comparable to that of the bounded width convolutional model. However, in Figure 4b, we observe that the energy spectrum of the adversarial perturbations for the ResNet model is more concentrated around middle frequencies (see also Supp. Figure 10). Taken together, these results serve as evidence *against* the hypothesis that ResNet models *unconditionally* exploit features with higher frequency than baseline Convnet models.

Frequency Spectra of VGG-19 & ResNet-18 show no difference compared to shallow models Given the previous results on ConvNet vs ResNet adversarial perturbations, we decided to circle back to the deep nonlinear models, whose adversarial perturbations originally sparked this study. For this, we trained a VGG-19 model on CIFAR10, and it achieved comparable performance to the ResNet-18 model (91% test accuracy). In Figure 4b, we observe that a small change in the radial energy distribution of the ResNet model toward higher frequencies. This result is opposite to the one shown for shallow ResNet, suggesting that depth could indeed have an effect on the implicit regularizer of ResNet models. Finally, we hypothesize that this small difference in the energy distribution could be further amplified by using a higher resolution dataset such as ImageNet, where the higher frequency perturbations were first observed.

The results for nonlinear models further support the implicit Fourier regularizer hypothesis, and a strong link between δ and β . Together these results strongly indicate that an implicit bias induced by convolutional operations strongly impacts the frequency-domain dynamics and nature of adversarial examples.

Conclusions and Future Work We probed the learning dynamics of adversarial examples, finding that they are not present at initialization, but that they emerge during training in order to model curvature, consistent with the Features-Not-Bugs hypothesis. We show that different parametrizations

and initialization schemes induce different implicit biases, which in turn, induce different kinds of energy spectra for adversarial examples. In particular, we demonstrate that the locality and translation invariance in convolutions induces an implicit bias towards sparsity in Fourier domain. This implicit bias, together with useful features in the dataset, is responsible for the low amplitude high frequency nature of commonly observed adversarial attacks. We anticipate that our work will help clarify the true nature of adversarial vulnerabilities, and thus guide us towards more robust and secure solutions.

Broader Impact

The potential beneficiaries of this work could be anyone who directly or indirectly utilizes neural networks for important or dangerous tasks e.g. self-driving cars, financial trading, medical diagnosis and prediction. By helping to elucidate the origin and root cause of adversarial sensitivity/vulnerability, we hope our work will enable the design of neural network models that are far more robust and secure. The only harm we can think of would accrue to those who wish to hack or spoof important systems with adversarial attacks.

We do not present a new system here so there is no risk of system failure. We use natural image data from the CIFAR-10 dataset, which do not contains any sensitive human data.

Acknowledgments

This research has been funded by the NSF NeuroNex program through grant DBI-1707400. This research was also supported by Intelligence Advanced Research Projects Activity (IARPA) via Department of Interior/Interior Business Center (DoI/IBC) contract number D16PC00003. The U.S. Government is authorized to reproduce and distribute reprints for Governmental purposes notwithstanding any copyright annotation thereon. Disclaimer: The views and conclusions contained herein are those of the authors and should not be interpreted as necessarily representing the official policies or endorsements, either expressed or implied, of IARPA, DoI/IBC, or the U.S. Government.

References

- [1] S. Arora, S. S. Du, W. Hu, Z. Li, R. R. Salakhutdinov, and R. Wang. On exact computation with an infinitely wide neural net. In *Advances in Neural Information Processing Systems*, pages 8139–8148, 2019.
- [2] S. Bubeck, E. Price, and I. Razenshteyn. Adversarial examples from computational constraints. *arXiv preprint arXiv:1805.10204*, 2018.
- [3] A. Fawzi, H. Fawzi, and O. Fawzi. Adversarial vulnerability for any classifier. In *Advances in Neural Information Processing Systems*, pages 1178–1187, 2018.
- [4] N. Ford, J. Gilmer, N. Carlini, and D. Cubuk. Adversarial examples are a natural consequence of test error in noise. *arXiv preprint arXiv:1901.10513*, 2019.
- [5] G. Gidel, F. Bach, and S. Lacoste-Julien. Implicit regularization of discrete gradient dynamics in linear neural networks. In *Advances in Neural Information Processing Systems*, pages 3196–3206, 2019.
- [6] J. Gilmer, L. Metz, F. Faghri, S. S. Schoenholz, M. Raghu, M. Wattenberg, and I. Goodfellow. Adversarial spheres. *arXiv preprint arXiv:1801.02774*, 2018.
- [7] G. Goh. A discussion of ‘adversarial examples are not bugs, they are features’: Two examples of useful, non-robust features. *Distill*, 2019. <https://distill.pub/2019/advex-bugs-discussion/response-3>.
- [8] I. J. Goodfellow, J. Shlens, and C. Szegedy. Explaining and harnessing adversarial examples. *arXiv preprint arXiv:1412.6572*, 2014.
- [9] S. Gunasekar, J. D. Lee, D. Soudry, and N. Srebro. Implicit bias of gradient descent on linear convolutional networks. In *Advances in Neural Information Processing Systems*, pages 9461–9471, 2018.

- [10] K. He, X. Zhang, S. Ren, and J. Sun. Deep residual learning for image recognition. In *Proceedings of the IEEE conference on computer vision and pattern recognition*, pages 770–778, 2016.
- [11] A. Ilyas, S. Santurkar, D. Tsipras, L. Engstrom, B. Tran, and A. Madry. Adversarial examples are not bugs, they are features. In *Advances in Neural Information Processing Systems*, pages 125–136, 2019.
- [12] A. Kurakin, I. Goodfellow, and S. Bengio. Adversarial examples in the physical world. *arXiv preprint arXiv:1607.02533*, 2016.
- [13] Z. Li, R. Wang, D. Yu, S. S. Du, W. Hu, R. Salakhutdinov, and S. Arora. Enhanced convolutional neural tangent kernels. *arXiv preprint arXiv:1911.00809*, 2019.
- [14] S. Mahloujifar, D. I. Diochnos, and M. Mahmoody. The curse of concentration in robust learning: Evasion and poisoning attacks from concentration of measure. In *Proceedings of the AAAI Conference on Artificial Intelligence*, volume 33, pages 4536–4543, 2019.
- [15] R. Nakano. A discussion of ‘adversarial examples are not bugs, they are features’: Adversarially robust neural style transfer. *Distill*, 2019. <https://distill.pub/2019/advex-bugs-discussion/response-4>.
- [16] P. Nakkiran. Adversarial robustness may be at odds with simplicity. *arXiv preprint arXiv:1901.00532*, 2019.
- [17] J. Rauber, W. Brendel, and M. Bethge. Foolbox: A python toolbox to benchmark the robustness of machine learning models. *arXiv preprint arXiv:1707.04131*, 2017.
- [18] E. Rusak, L. Schott, R. Zimmermann, J. Bitterwolf, O. Bringmann, M. Bethge, and W. Brendel. Increasing the robustness of dnns against image corruptions by playing the game of noise. *arXiv preprint arXiv:2001.06057*, 2020.
- [19] J. Sahs, A. Damaraju, R. Pyle, O. Tavaslioglu, J. O. Caro, H. Y. Lu, and A. Patel. A functional characterization of randomly initialized gradient descent in deep re{lu} networks, 2020.
- [20] L. Schmidt, S. Santurkar, D. Tsipras, K. Talwar, and A. Madry. Adversarially robust generalization requires more data. In *Advances in Neural Information Processing Systems*, pages 5014–5026, 2018.
- [21] A. Shafahi, W. R. Huang, C. Studer, S. Feizi, and T. Goldstein. Are adversarial examples inevitable? *arXiv preprint arXiv:1809.02104*, 2018.
- [22] T. Tanay and L. Griffin. A boundary tilting persepective on the phenomenon of adversarial examples. *arXiv preprint arXiv:1608.07690*, 2016.
- [23] D. Tsipras, S. Santurkar, L. Engstrom, A. Turner, and A. Madry. Robustness may be at odds with accuracy. *arXiv preprint arXiv:1805.12152*, 2018.
- [24] F. Williams, M. Trager, D. Panozzo, C. Silva, D. Zorin, and J. Bruna. Gradient dynamics of shallow univariate relu networks. In *Advances in Neural Information Processing Systems*, pages 8376–8385, 2019.
- [25] B. Woodworth, S. Gunasekar, J. D. Lee, E. Moroshko, P. Savarese, I. Golan, D. Soudry, and N. Srebro. Kernel and rich regimes in overparametrized models. *arXiv preprint arXiv:2002.09277*, 2020.
- [26] C. Xie, M. Tan, B. Gong, J. Wang, A. Yuille, and Q. V. Le. Adversarial examples improve image recognition. *arXiv preprint arXiv:1911.09665*, 2019.
- [27] D. Yin, R. G. Lopes, J. Shlens, E. D. Cubuk, and J. Gilmer. A fourier perspective on model robustness in computer vision. In *Advances in Neural Information Processing Systems*, pages 13255–13265, 2019.

A Additional Figures & Tables

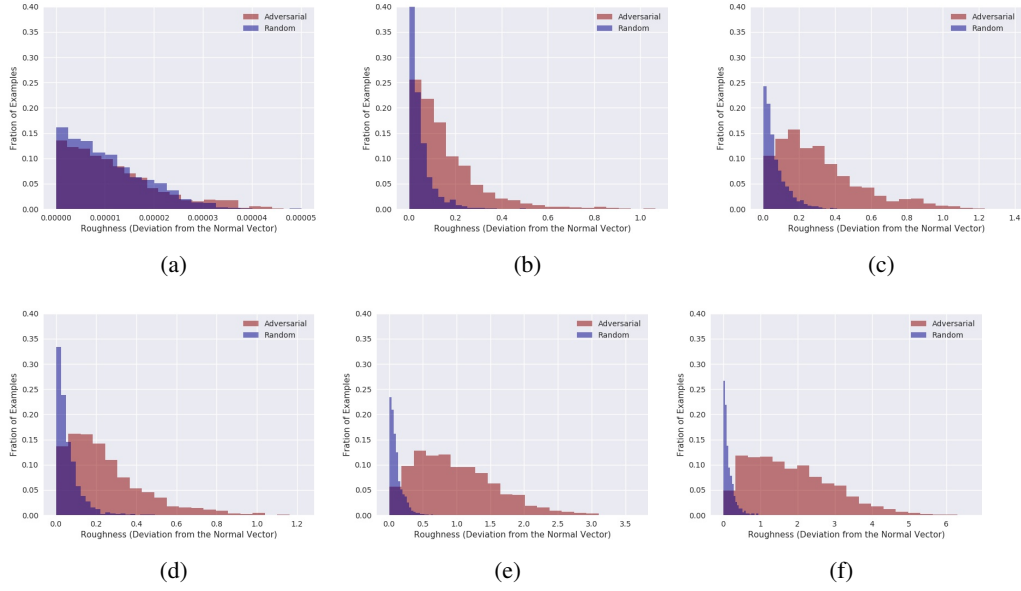


Figure 6: Distribution of Roughness (Metric for Curvature) for epochs 0,5,10,20,25,40 (a,b,c,d,e,f respectively) for ResNet18 Model with x_a and x_r perturbations. See that Roughness starts the same for both perturbations, but increase more at the end of training for the Adversarial perturbations.

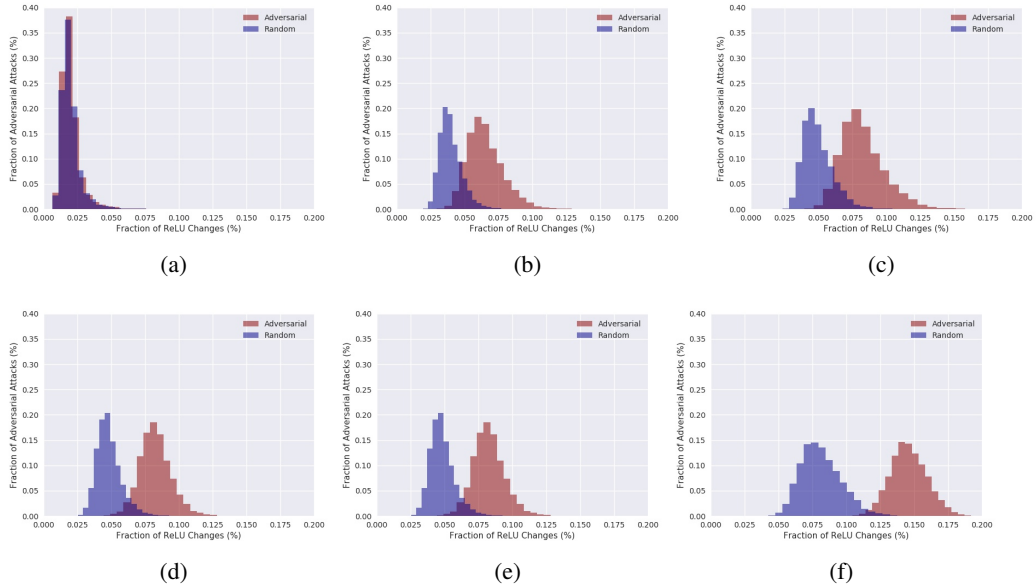


Figure 7: Distribution of Fraction of ReLU Changes for epochs 0,5,10,20,25,40 (a,b,c,d,e,f respectively) for ResNet18 Model with x_a and x_r perturbations. See that fraction of ReLU Changes starts the same for both perturbations, but increase more at the end of training for the Adversarial perturbations.

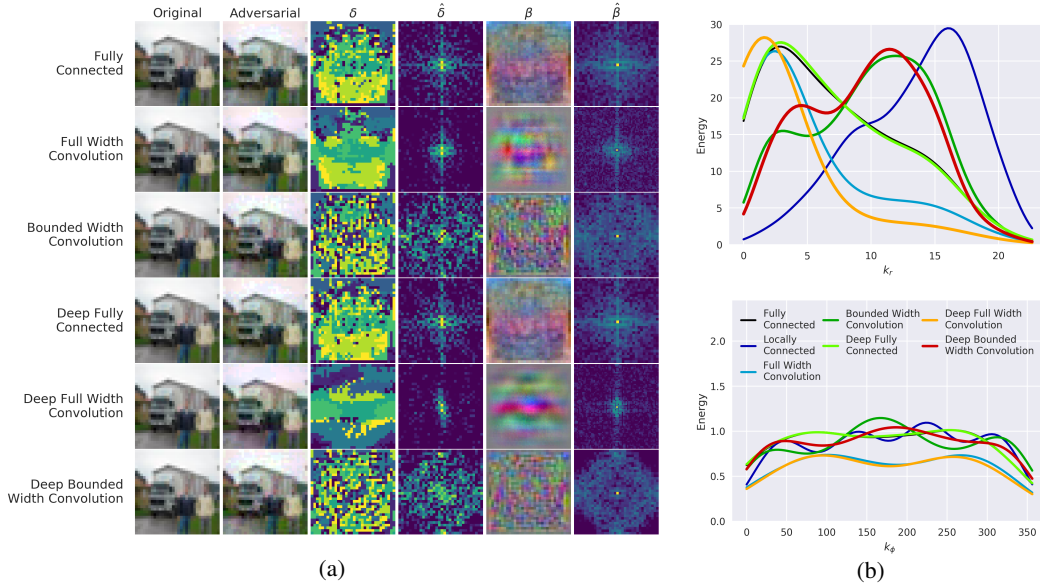


Figure 8: (a) Example Visualization of δ , $\hat{\delta}$, β and $\hat{\beta}$ for 6 overparametrized linear models with one hidden layer. We observe qualitatively (particularly in $\hat{\beta}$) that both full width and bounded width convolutional models are sparser than the Fully Connected model. For quantification, see Table 1. (b) Top: Distribution of energy along in fourier spectrum

Model	$\ \hat{\delta}\ _2$	$\ \hat{\delta}\ _1$	$\ \hat{\beta}\ _2$	$\ \hat{\beta}\ _1$
Fully Connected	20.77 ± 1.23	505.95 ± 32.22	546.89 ± 43.37	2232.46 ± 166.27
Full Width Convolution	17.52 ± 1.56	376.31 ± 32.66	544.83 ± 42.40	1598.37 ± 181.44
Bounded Width Convolution	20.65 ± 1.09	556.32 ± 32.64	500.67 ± 47.46	2623.04 ± 331.42
Deep Fully Connected	20.83 ± 1.25	503.92 ± 32.62	554.16 ± 38.95	2168.06 ± 134.07
Deep Full Width Convolution	17.13 ± 1.68	265.40 ± 41.72	522.99 ± 39.72	1417.68 ± 213.91
Deep Bounded Width Convolution	20.57 ± 0.94	550.30 ± 29.71	498.52 ± 47.15	2392.09 ± 278.55

Table 1: Frequency-Domain Norms of Predictor $\hat{\beta}$ and Adv. Pert. $\hat{\delta}$ for Linear Models. With Equivalent performance (See Sup Figure 4), Convolutional Models have smaller $\|\hat{\beta}\|_1$, supporting the implicit Fourier hypothesis.

Model	$\ \hat{\delta}\ _2$	$\ \hat{\delta}\ _1$
Fully Connected	22.06 ± 1.35	534.34 ± 35.93
Locally Connected	22.32 ± 1.13	587.61 ± 29.89
Full Width Convolution	20.57 ± 1.11	405.49 ± 34.16
Bounded Width Convolution	24.63 ± 1.36	665.22 ± 38.55
Shallow ResNet	26.36 ± 0.74	709.06 ± 20.76
VGG19	23.32 ± 0.99	650.73 ± 27.87
ResNet18	22.42 ± 0.91	626.60 ± 25.40

Table 2: Frequency-Domain Norms of Adv. Pert. $\hat{\delta}$ for Nonlinear Models. With similar performance (Supp. Table 1), Full Width and Bounded Width convolutional models produce adversarial attacks with smaller $\|\hat{\delta}\|_1$.

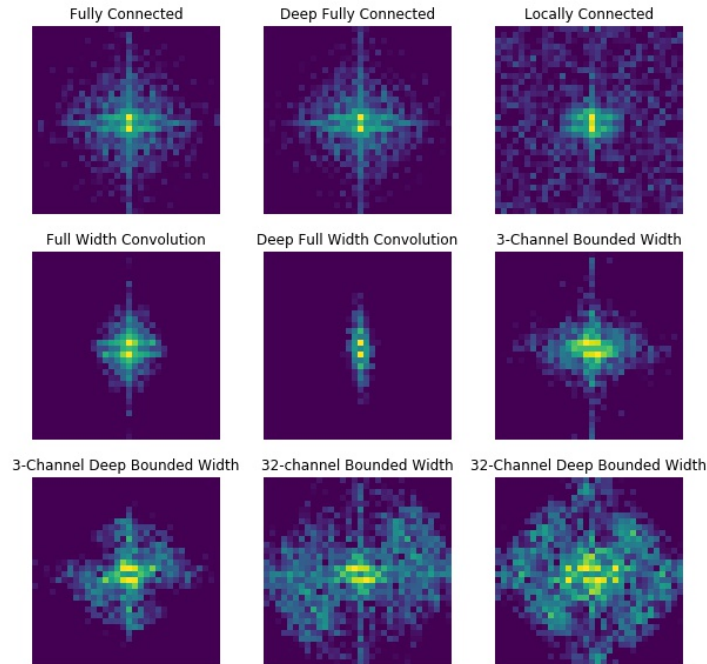


Figure 9: Visualization of the average of the spectra $\widehat{\delta}_n$ over all sampled inputs n for all linear models. The average spectra are similar to those observed in Figure 8.

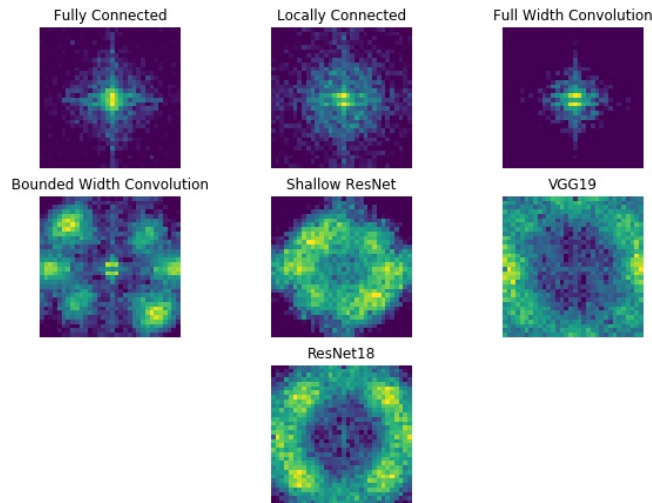


Figure 10: Visualization of the average of the spectra $\widehat{\delta}_n$ over all sampled inputs n for all nonlinear models. The average spectra are similar to the examples observed in Figure 4

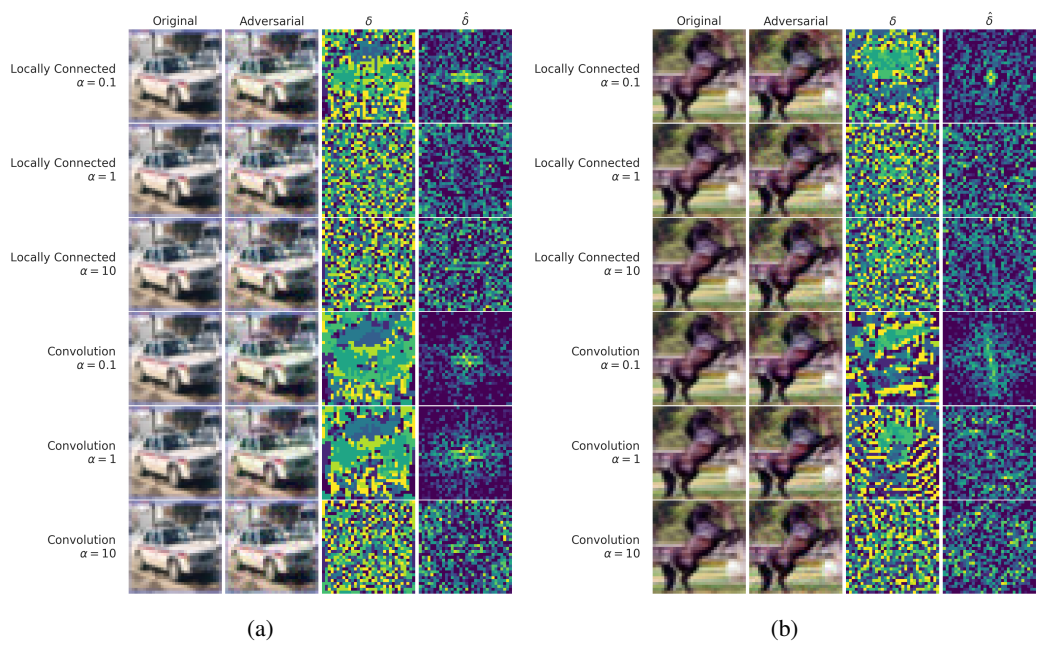


Figure 11: (a) The impact of initial weight scale α on the adversarial spectrum of linear models. Higher α induces higher frequency spectra for both locally connected and convolutional models. (b) The impact of initial weight scale α on the adversarial spectrum of *nonlinear* models. Higher α induces higher frequency spectra for both locally connected and convolutional models.

B Experimental Details

B.1 Model Architectures

Model Architecture	# Hidden Layers	Nonlinearity	Channels
Fully Connected	1,3	None, ReLU	2700
Bounded Width Convolution	1,3	None, ReLU	(3,32)
Full Width Convolution	1,3	None, ReLU	3
Locally Connected	1	None, ReLU	32

Table 3: Model Architectures

B.2 Model Performance

Model Architecture	Test Accuracy
Fully Connected (Linear)	41%
Locally Connected (Linear)	35%
Full Width Convolution (Linear)	41%
Bounded Width Convolution (Linear)	41%
Deep Fully Connected (Linear)	41%
Deep Full Width Convolution (Linear)	36%
Deep Bounded Width Convolution (Linear)	41%
Fully Connected (NonLinear)	52%
Locally Connected (NonLinear)	54%
Bounded Width Convolution (NonLinear)	63%
Shallow ResNet (NonLinear)	64%
VGG19	91%
ResNet18	92%

Table 4: Test Accuracy for all models trained. All linear models have similar performance. Nonlinear models exhibit more variability.

B.3 Training Hyperparameters

Model Architecture	Learning Rate	Batch Size	Learning Rate Drop
Bounded Width Convolution	.01	128	Yes
Fully Connected	.01	128	Yes
Locally Connected	.01	128	Yes
Full Width Convolution	.002	128	Yes
Bounded Width Convolution	.002	128	Yes

Table 5: Learning rates for the various models considered. All other hyper-parameters were fixed.

Learning Rates. We tuned the max learning rates for each model by starting from a base learning rate of 0.1, and then, if there were visible failures during training (most commonly, the model converging to chance performance), we adjusted the learning rate up/down by a factor of 10 or 50.

Amongst the model architectures we explored, the only hyper-parameter that was tuned was the learning rate. The final values of the learning rates after search are detailed in Table 5.

In addition, all the models were trained with linearly decaying learning rate follow 0.3 factor for each epoch and resetting the learning rate back to max when you trained the model at least 20 epochs. All models were trained for at least 40 epochs and we choose the epoch with the highest accuracy for further experiments.

Attack	Metric	Learning Rate	Number of Steps	Max Norm, ϵ
Projected Gradient Descent	L_∞	0.1	1000	8.0/255.0

Table 6: Adversarial Attack hyperparameters

B.4 Adversarial Attack Configurations

Learning Rates. All the models adversarial attacks were generated using the configuration above with the Foolbox package [17].